Science of the Total Environment 957 (2024) 177597

Contents lists available at ScienceDirect

Science of the Total Environment

journal homepage: www.elsevier.com/locate/scitotenv

Mechanistic insights into the co-transport of microplastic degradation products in saturated porous media: The key role of microplastics-derived DOM

Kaixuan Sun [a], Xiaofeng Huo [b], Yanhong Zhang [b,*], Chengyuan Zong [c], Chao Liu [a], Zhanxue Sun [a], Xiaoxia Yu [a,*], Peng Liao [d]

[a] Jiangxi Provincial Key Laboratory of Genesis and Remediation of Groundwater Pollution, East China University of Technology, Nanchang 330013, Jiangxi, PR China
[b] School of Water Resources and Environmental Engineering, East China University of Technology, NanChang 330013, Jiangxi, PR China
[c] Zhejiang Environmental Technology Co., Ltd, Hangzhou, 310012, PR China
[d] State Key Laboratory of Environmental Geochemistry, Institute of Geochemistry, Chinese Academy of Sciences, Guiyang, 550081, PR China

HIGHLIGHTS

- The typical transport order under various environmentally relevant conditions was MP-DOM > AMPs > OMPs in this study.
- As the aging degree increases, MP-DOM becomes increasingly important in the co-transport of secondary products.
- MP-DOM provides a rising TOC proportion, high mobility, and the ability to facilitate the migration of MPs.
- MP-DOM affected the transport of MPs through a combination of positive and negative effects.

GRAPHICAL ABSTRACT

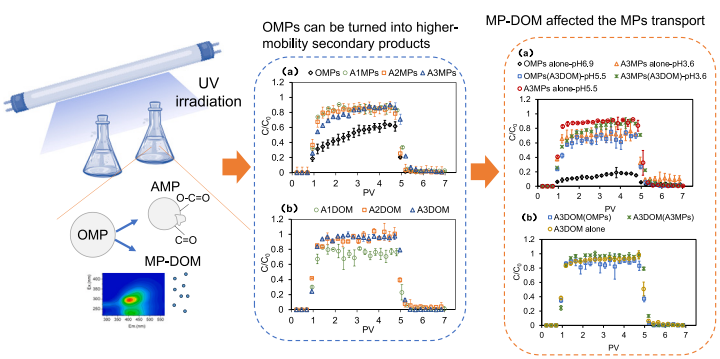

ARTICLE INFO

Editor: Damià Barceló

Keywords:
Microplastic degradation products
Microplastics-derived DOM
Co-transport
Porous media
Aging

ABSTRACT

Microplastic-derived dissolved organic matter (MP-DOM) forms from the aging of microplastics (MPs), but the co-transport behavior of MP-DOM and aged MPs (AMPs) remains poorly understood. This study investigates the co-transport of AMPs and MP-DOM generated from original MPs (OMPs) over a wide range of environmentally relevant conditions. The transport of AMPs and MP-DOM changes as the degree of aging increases, specifically related to changes in their physicochemical characteristics. Results showed that the order of migration ability was MP-DOM > AMPs > OMPs under almost all tested conditions. The change of hydrophobicity of MP-DOM and AMPs, as well as small molecular weight of MP-DOM, was primarily responsible for this order. The role of MP-DOM as a degradation product in the co-transport process is notably significant under various environmental conditions because of its high mobility and organic carbon fraction within the system. Furthermore, it is important to note that MP-DOM affected the transport of MPs through a combination of positive and negative effects. Key mechanisms include electrostatic repulsion caused by protonation reactions triggered by the acidic

* Corresponding authors.
E-mail addresses: 201660015@ecut.edu.cn (Y. Zhang), yuxiaoxiayxx@126.com (X. Yu).

https://doi.org/10.1016/j.scitotenv.2024.177597
Received 19 September 2024; Received in revised form 10 November 2024; Accepted 14 November 2024
Available online 28 November 2024

pH of MP-DOM, steric hindrance, and competition for retention sites on media surfaces. This study contributes to a deeper understanding of the transformation and fate of MPs in complex environmental systems.

1. Introduction

Microplastics pollution in soil has received significant attention due to the substantial discharge of plastic waste directly into terrestrial ecosystems (Castan et al., 2021). By 2050, it is projected that global plastic waste generation will reach 26,000 Mt., with at least 45 % of this expected to remain unrecycled and unincinerated (Geyer et al., 2017). Microplastics in natural environments can undergo various weathering processes, such as light-induced degradation, biodegradation, and mechanical degradation, which facilitate the release of aged microplastics (AMPs) and dissolved organic matter associated with MP (MP-DOM) (Lee et al., 2020; Thompson et al., 2004). Both MPs and MP-DOM contain substantial amounts of organic carbon that can participate in nutrient and carbon cycling (Rillig, 2018; Rillig et al., 2021; Sun et al., 2022). Furthermore, MPs and MP-DOM can inhibit organism growth, alter crucial biological processes like carbon transformation, and exacerbate the climate crisis by releasing greenhouse gases (Shi et al., 2021; Zhou et al., 2023).

Weathering process causes severe damage to the structure and surface characteristics of MP that include size, hydrophobicity, morphology, and functional groups (Wang et al., 2023). Concurrently, continuous chain scission reactions produce a diverse array of MP-DOM comprising thousands of molecular formulas such as low-molecular weight organic additives and broken polymer products (Gewert et al., 2018; Kwon et al., 2015; Lee et al., 2023). Notably, the weathering process leads to the continual aging of MPs and MP-DOM, which manifests as dynamic changes in their composition and properties. Liu et al. (2019b) reported that during aging of polystyrene (PS), its surfaces roughness and amount of nano-debris increase, along with greater degrees of surface oxidation and hydrophilicity. Similarly, Ren et al. (2023) found that the components of DOM released from PVC and PS shift from high-molecular-weight fractions to low-molecular fractions with aging, and their chromogenic components of DOM continually change. Consequently, the environmental behavior of MPs and MP-DOM is likely to be continually evolving. However, research on this dynamic aspect is limited, which hampers a thorough assessment of the environmental impacts throughout the entire life cycle of MPs degradation.

Furthermore, although AMPs and MP-DOM are two types of products produced simultaneously during the aging process, most of the existing researches focused primarily on their individual functions, and there is a lack of knowledge regarding their joint functions, particularly their co-transport propensity in porous media. Many studies have found that the transport of MPs in porous media is influenced by human activities (e.g., plowing and harvesting), bioturbation, MPs properties, co-existing substances (e.g., heavy metal, organic matter, nanoparticles), and environmental factors (e.g., porosity, soil pH, ionic strength (IS), cation type, mineral contents, wet-dry cycles, and flow rate) (Ren et al., 2021a; Ren et al., 2021b; Xi et al., 2022). In contrast, fewer studies have examined the co-transport of MP-DOM, which is a heterogeneous and complex mixture, in conjunction with MPs. MP-DOM is not merely a collection of oligomers, monomers, and functional additives; it often contains the byproducts and intermediates formed during various degradation or aging processes. Based on the excitation-emission matrix and parallel factor analysis, MP-DOM samples exhibit the most prominent protein/phenol-like and humic-like fluorescence (Lee et al., 2021; Ouyang et al., 2023). According to Fourier transform ion cyclotron resonance mass spectrometry analysis, MP-DOM includes labile carbon molecules such as lipid-like, protein/amino sugar-like, and carbohydrate-like compounds (Sun et al., 2022). It has been suggested that the MP-DOM released from UV-aging MPs had the ability to readily transport into the pore water of sandy subsurface system. Additionally, different MP-DOM components respond variably to environmental interferences, with protein/phenol-like C2 being more sensitive to biodegradation and mineral adsorption than humic-like C1 (Lee et al., 2022). MP-DOM contains various low-molecular-weight organic acids (LMWOAs) (Gewert et al., 2018). Some of these LMWOAs that are ubiquitous in the environment, such as acetic acid, citric acid, and cinnamic acid, can substantially enhance the transport of biochar nanoparticles, graphite oxide, and microplastics (Li et al., 2019; Zhang et al., 2024a; Zhang et al., 2024b). A recent study has also reported that the intermediates from the photo-Fenton oxidation of polystyrene (PS) can adsorb onto PS and increase its negative charges, thereby influencing their electrostatic forces (Liu et al., 2020). MP-DOM may exhibit similar functionalities to LMWOAs, and MPs may act as a carrier for MP-DOM cotransport. However, the absence of research on the co-transport of MPs and MP-DOM limits our understanding of the transformation and ultimate fate of MPs in complex systems.

The overarching goal of this study is to investigate the co-transport of the MP's degradation products of MP-DOM and aged MPs in saturated porous media. To this end we designed experiments under a wide range of environmentally relevant conditions that may potentially influence the co-transport of MPs and MP-DOM (Fei et al., 2022; Li et al., 2019; Ren et al., 2021a). PS was selected for photo-aging experiments due to its ubiquitous in soils and associated risks (Siddiqui et al., 2023). The specific objectives are: (1) to clarify the transport behavior of degradation products with varying degree of aging; (2) to compare and determine the contributions and mechanisms of MP-DOM and MPs co-transport under varying conditions, including different ionic strength (IS), cation type, grain size, and medium type.

2. Materials and methods

2.1. Preparation of MPs and MP-DOM

Submicron monodisperse PS microplastics (used as original MPs, OMPs) with a diameter of 505 ± 10 nm (data was provided by the manufacturer), were purchased from Ganzhou Mxene Technology Co., Ltd. (Ganzhou, China). The original concentration of the OMPs suspension is 50 g/L (5 % *W/V*). Further information on the preparation and properties of other materials can be found in Text A1 of the Appendices.

MPs with different aging degrees and the concurrent release of MP-DOM were collected by subjecting OMPs to UV irradiation in DI water. To prepare AMPs and MP-DOM mixtures, aging test was applied in lighting chamber equipped with ultraviolet (UV) lamps (500 W mercury lamps). UV irradiation has been intensively used to accelerate MPs aging as an artificial method since most of the MPs were sensitive to UV light in the sunlight (Gewert et al., 2018). The OMPs suspension at 50 g/L was diluted to 100 mg C/L using DI water, following sonication for 30 min to ensure thorough dispersion. Then, the diluted suspension was added to a quartz jar and subjected to UV-irradiation at 26 ± 2 °C with an intensity of 4.6 mW/cm^2 until the concentration of aged MPs and MP-DOM reached a predetermined level. The concentrations (mg C/L) of MPs and MP-DOM in suspensions were detected using a TOC analyzer (TOC-L CPH CN200, Shimadzu, Japan) which is capable of analyzing suspensions containing uniformly suspended particles. Specifically, the total TOC of mixtures including MPs and MP-DOM were determined first. Subsequently, the filtrates containing only MP-DOM (obtained through a 10 kDa ultrafiltration membrane) were analyzed. The difference in TOC between the total suspension and the filtrate was considered to represent the TOC of MPs (Text A2).

During this period, the UV energy received at the sample position,

the concentration of MPs, and the volume of suspensions all affect the degree of MPs aging. To standardize the aging degree, the criteria used were aging time, the concentration (mg C/L), and ratio of aged MPs to MP-DOM. For consistency, each time, 200 mL of a 100 mg C/L PS suspension was irradiated under these conditions. Column experiments were conducted with three different aging degrees of MPs and MP-DOM mixtures (Table 1). The following ratios of MP-DOM concentration (mg C/L) to aged MPs concentration (mg C/L) and corresponding aging times were used: 1: 5 (A1DOM: A1MPs), aging for 15 h; 1: 2.5 (A2DOM: A2MPs), aging for 25 h; and 1: 1 (A3DOM: A3MPs), aging for 38 h.

2.2. Analytical methods

2.2.1. MPs

The surface morphology and element abundance of PS MPs were characterized by SEM-EDS (SEM: Sigma 300, ZEISS, Germany; EDS: Smartedx, ZEISS, Germ ration The size distributions and average size of MPs particles were determined by measuring particles in SEM images using Nano measurer software (Version 1.2.5, Fudan University) (Liu et al., 2022). The ζ-potentials of MPs were determined using a Zetasizer (Nano ZS90, Malvern, England). FTIR spectroscopy of the MPs were obtained using a Thermo Scientific Nicolet iS20 spectrometer (Thermo Nicolet Co., Madison, US).

2.2.2. MP-DOM

Fluorescence excitation emission matrices (EEMs) were obtained using a spectrofluorophotometer (F-7000, Hitachi, Japan), and PARAFAC modeling was performed using MATLAB 7.0 (Mathworks Inc., US) with drEEM Toolbox (Text A3). The FTIR was used to identify the functional groups in the filtrate samples (Text A4). Ten low-molecular weight chemicals (Table A1) were analyzed using Ultra performance liquid chromatography quadrupole time-of-flight mass spectrometry (UPLC-Q-TOF MS, UPLC1290 equipped with QTOF 6550, Agilent, US) to quantify products derived from UV-aging PS (Text A5). The quantitative analysis (mg C/L) was detailed in Text A2. Contact angle (CA) between MP-DOM solution and quartz plate simulating quartz sand was measured by a contact angle meter (JC-2000CI, Shanghai Zhongchen Digital Technology Equipment Co., Ltd., China).

2.3. Column experiments

All column experiments were conducted in duplicate. Quartz sand or limestone was wet-packed into the acrylic columns (length: 16.8 cm, diameter: 2.5 cm) with 30 μm stainless-steel screens on both ends. The constant upward flow rate of 1.0 mL/min was controlled by peristaltic pump (BT100-1F, Longer Pump, China). All packed column porosities are shown in Table 2. Prior to each experiment, the column was flushed with DI water for 10 pore volumes (PVs). To equilibrate the pore water IS and pH, the system was flushed with the background electrolyte solution for 10 PVs. This solution had the same pH, ionic type, and IS as the working suspensions, but did not contain MPs or MP-DOM. Subsequently, 4 PVs of working suspension (MPs suspension with different aging degrees prepared in an electrolyte solution, see Table 2) was injected into columns, followed by a subsequent injection of 2 PVs of background electrolyte solution. The effluent samples were collected by fraction collectors (BS-100 A, Shanghai Huxi Analysis Instrument Factory CO., LTD, China) every 8 min to determine MPs and MP-DOM concentrations (same as described in Section 2.1). For all column experiments, including limestone columns, the cations and pH in effluents were stabilized before injecting working solution. The overall effluent pH values of limestone columns ranged between 7.4 and 7.6 due to the buffering capacity of limestone, whereas the pH values of sand columns were comparable to the influent.

Table 1
The concentrations of MPs and MP-DOM in the four samples used in the column experiments.

Name	Total TOC concentrations of the mixtures with different UV-aging degrees (mg C/L)	TOC concentrations of OMPs to AMPs (mg C/L)	TOC concentrations of MP-DOM (mg C/L)	The ratio of MP-DOM (mg C/L) to AMPs (mg C/L)
O-system	29.1 ± 0.4	29.1 ± 0.4	–	–
A1-system	29.8 ± 0.0	25.0 ± 0.4	4.7 ± 0.4	1:5
A2-system	29.3 ± 0.3	20.8 ± 0.4	8.4 ± 0.0	1:2.5
A3-system	29.7 ± 0.6	14.7 ± 0.8	15.0 ± 0.7	1:1

O-system, A1-system, A2-system, A3-system: the four samples we used in column experiments. In this study, the total organic carbon concentrations of the four samples in the influent were set to be consistent. O-system only has original MPs. The A1-system, A2-system, and A3-system have UV-aging products, including aged MPs and MP-DOM. When the latter three mixtures diluted to the same total TOC concentration, their respective AMPs (mg C/L): MP-DOM (mg C/L) ratios were about 1: 5 (A1DOM: A1MPs), 1: 2.5 (A2DOM: A2MPs), 1:1 (A3MPs: A3DOM).
Conc.: concentration.
–: There is no such item.

Table 2
Summary of experimental conditions for packed column experiments.

Column NO.	Media type (grain size, mm)	Porosity	Influent	Electrolytic conc. (mM)		Ionic strength (mM) [a]	Effluent recovery rate (ERR) (%) [b]	MPs or MP-DOM (mg C/L)/[MPs + MP-DOM] (mg C/L) (%) [c]
				NaCl	$CaCl_2$			
1	Quartz sand (0.425–0.600)	0.41	O-system	1	0	1	MPs: 51.0 ± 3.9	–
2	Quartz sand (0.425–0.600)	0.41	O-system	3	0	3	MPs: 5.7 ± 0.6	–
3	Quartz sand (0.425–0.600)	0.40	O-system	9	0	9	MPs:0	–
4	Quartz sand (0.425–0.600)	0.41	O-system	0	0.33	1	MPs: 18.1 ± 0.1	–
5	Quartz sand (0.425–0.600)	0.40	O-system	0	1	3	MPs: 0	–
6	Quartz sand (0.425–0.600)	0.40	O-system	0	3	9	MPs: 0	–
7	Quartz sand (0.250–0.355)	0.35	O-system	1	0	1	MPs:0	–
8	Quartz sand (0.700–0.850)	0.42	O-system	1	0	1	MPs: 83.3 ± 1.8	–
9	Limestone (0.425–0.600) LS (M) [g]	0.41	O-system	1	0	1	MPs: 6.0 ± 0.5	–
10	Quartz sand (0.425–0.600)	0.41	A1-system	1	0	1	MPs: 83.2 ± 2.1 DOM: 79.8 ± 4.1	71.05 ± 0.01 13.41 ± 0.75
11	Quartz sand (0.425–0.600)	0.41	A2-system	1	0	1	MPs: 83.2 ± 0.1 DOM: 97.4 ± 2.7	59.33 ± 0.07 28.01 ± 0.77
12	Quartz sand (0.425–0.600)	0.42	A3-system	1	0	1	MPs: 81.2 ± 0.9 DOM: 95.2 ± 1.0	42.47 ± 0.53 45.44 ± 0.50
13	Quartz sand (0.425–0.600)	0.40	A3-system	3	0	3	MPs: 76.9 ± 2.0 DOM: 93.9 ± 1.6	34.64 ± 0.91 51.59 ± 0.87
14	Quartz sand (0.425–0.600)	0.41	A3-system	9	0	9	MPs: 60.8 ± 0.3 DOM: 93.7 ± 1.4	29.32 ± 0.16 48.56 ± 0.72
15	Quartz sand (0.425–0.600)	0.41	A3-system	0	0.33	1	MPs: 77.1 ± 0.6 DOM: 96.2 ± 0.4	39.81 ± 0.51 46.69 ± 0.21
16	Quartz sand (0.425–0.600)	0.41	A3-system	0	1	3	MPs: 59.9 ± 1.5 DOM: 91.8 ± 0.7	32.02 ± 0.80 42.77 ± 0.34
17	Quartz sand (0.425–0.600)	0.41	A3-system	0	3	9	MPs: 31.8 ± 0.6 DOM: 98.0 ± 1.2	15.33 ± 0.27 50.86 ± 0.63
18	Quartz sand (0.250–0.355)	0.34	A3-system	1	0	1	MPs: 3.7 ± 2.2 DOM: 55.8 ± 4.5	1.62 ± 0.94 29.26 ± 2.34
19	Quartz sand (0.700–0.850)	0.41	A3-system	1	0	1	MPs: 85.8 ± 3.0 DOM: 92.8 ± 1.8	38.75 ± 0.79 47.37 ± 0.93
20	Limestone (0.425–0.600)	0.41	A3-system	1	0	1	MPs: 8.3 ± 1.4 DOM: 83.8 ± 0.8	4.69 ± 0.08 41.23 ± 0.37

[a] $I = \frac{1}{2}\sum_{i=0}^{n} m_i \nu_i^2$. I is the ionic strength (mM L^{-1}); m_i is the concentration of ion (mM L^{-1}) and ν_i is the charge of the ion.
[b] The ratio of MPs or MP-DOM mass (mg C/L) in the effluent to MPs or MP-DOM mass (mg C/L) in the influent.
[c] The ratio of MPs or MP-DOM mass (mg C/L) in the effluent to MPs and MP-DOM mass (mg C/L) in the influent.

3. Results and discussion

3.1. The effect of aging on the degradation products of MPs

3.1.1. Characterization of MPs and MP-DOM

The shape and surface smoothness of aged MPs were similar to those of OMPs, though slight nano-debris was observed on aged MPs surfaces (Fig. 1a). Significant changes were noted in the average size and size distribution of MPs in UV-aging process (Fig. 1b and Table A2). Despite minor differences between Nano ZS90 and SEM data, both methods consistently showed a decrease in average diameters of MPs particles with increasing UV aging. Specifically, the proportion of MPs with size ≥500 nm decreased to 77.7 % (A1MPs), 2.27 % (A2MPs), and 0 (A3MPs), while the proportion of smaller MPs increased. EDS analysis (Fig. A1(a)) showed a gradual increase in O content with UV aging (wt% from 15.85 to 30.92). For both OMPs and AMPs, the adsorption peaks at 698, 836, and 3026 cm^{-1} were attributed to the aromatic C—H bending, while peaks at 1492 cm^{-1} were attributed to the C═C stretching of aromatic ring. The aged MPs exhibited additional bands such as C═O/O-C═O stretching bands at 1720–1722 cm^{-1} (Fig. 1c), indicating an increase in hydrophilic functional groups and polarity (Liu et al., 2019b). The zeta potential of MPs become more negative with increasing aging degree, decreasing from – 43.0 to – 54.8 mV (Table A3). This shift is consistent with higher O/C ratios and increased oxygen-containing functional groups, as also reported by Ren et al. (2021a).

The UV-aging kinetic experiments (Text A6 and Fig. A1) showed that the MP-DOM in filtrate increased from 0 to 35.2 mg C/L, and then decreased to 20.6 mg C/L within 63 h, while the MPs dropped from ~100 to 0 mg C/L. This decline was due to the release of MP-DOM and further mineralization under continuous UV exposure (Tian et al., 2019). The pH of leachates from the O, A1, A2, and A3 system were 6.95, 3.95, 3.69, and 3.50, respectively, indicating the formation of acidic substances (e.g., -COOH), which increased with UV-aging. For A1-A3DOM, the C=O/O-C=O stretching bands at 1713–1724 cm^{-1} and C—O peaks at 1090 cm^{-1} intensified with UV-aging (Fig. 2a). The distributions of monitoring compounds varied across A1-A3DOM (Fig. 2b and Table A4), with many compounds remaining unidentified, suggesting a diversity organic byproducts. The number of detected chemicals increased with UV-aging, and compounds with -COOH and -COO- groups become more prevalent. The fluorescence EEM spectra of A1-A3DOM (Fig. 2c-e) showed differences, and the PARAFAC model identified three different fluorescent components (C1, C2, and C3) (Fig. S3) with peak fluorescence at 230(290)/405, 250(320)/445, and (⟨220) 270/305 nm respectively, corresponding to humic-like (C1 and C2) and protein/phenol-like components (C3) (Lee et al., 2020; Wang et al., 2023). Overall, the photoluminescence intensities increased slightly (Fig. 2c), with an increase in humic-like substances and a decrease in protein/phenol-like components (Fig. 2d-e), likely due to the preferential degradation of phenolic degradation products which are more susceptible to UV oxidation (Wang et al., 2023).

3.1.2. Changes in the transport of MPs and MP-DOM

The transport of four MPs systems (O, A1, A2 and A3) with varying degrees of aging was investigated separately. As shown in Fig. 3 and Table 1 (column NO.1, 10–12), the transport of MP-DOM (ERR: 95.2 % ~ 97.4 %) was greater compared to AMPs (ERR: 81.2 % ~ 83.2 %) in A2 and A3 systems. However, in the A1 system with the weakest aging degree, the order is reversed (ERR: 79.8 % of MP-DOM and 83.2 % of

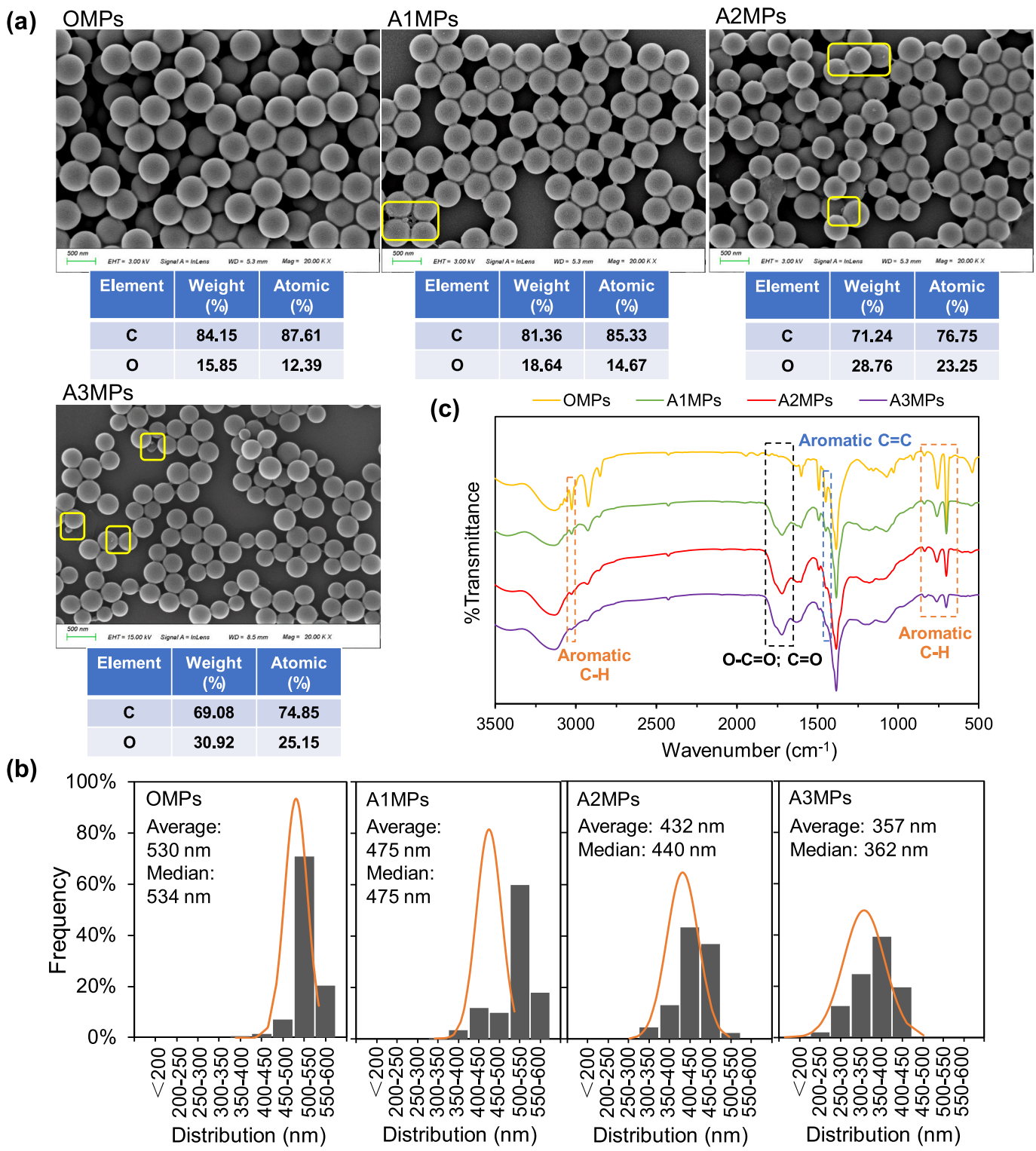

Fig. 1. SEM (Mag = 20.00 k x) and element analysis (the yellow boxes showed few nano-debris or crack parts observed) (a); size distribution (analyzed by Nano measurer 1.2.5) (b) and FTIR spectra (c) of OMPs, A1MPs, A2MPs and A3MPs.

MPs). All MP-DOM and AMPs demonstrated higher mobility than OMPs (ERR: 51.0 %), indicating that OMPs can be transformed into higher-mobility secondary products during UV aging.

Although MPs' transport increased significantly with aging, no notable differences were observed among the three aging degrees for AMPs. The stronger electrostatic repulsion between negatively charged particles and negatively charged sand grains within porous media is recognized as one of the dominant mechanisms for MPs transport (Li et al., 2023; Xi et al., 2022) (Table A3). However, this cannot fully explain the increased mobility of AMPs. The zeta potential of A1MPs (−44.7 mV) and OMPs (−43.0 mV) showed no distinct differences compared to A2MPs (−51.2 mV) and A3MPs (−54.8 mV). Notably, the pH of A1-A3 systems ranged from 3.50 to 3.95. The acidic pH is generally not conducive to the mobility of MPs (Fei et al., 2022).

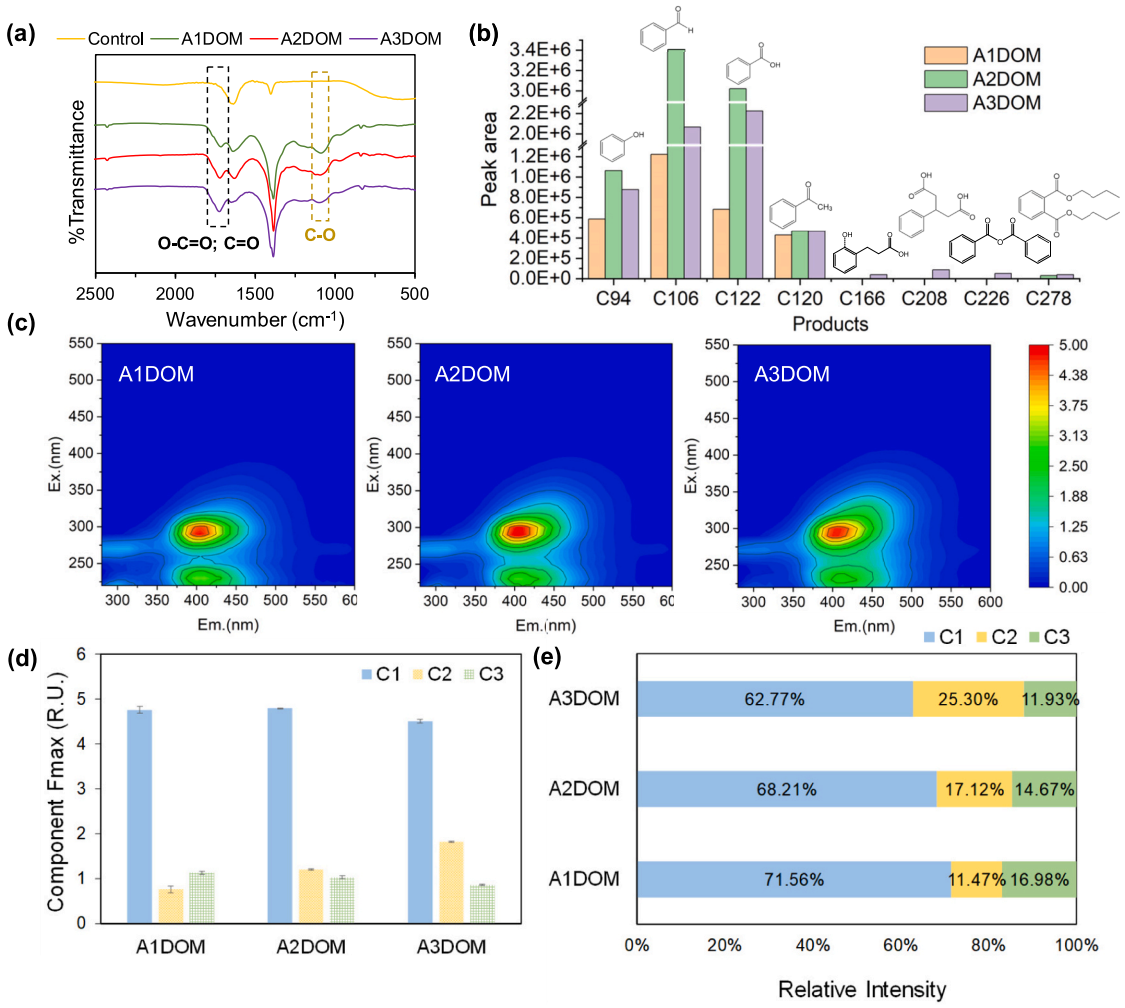

Fig. 2. FTIR spectra (a), photo-transformation products (specific peak area) (b) and Fluorescence EEM plots of A1DOM, A2DOM and A3DOM; (d) Fmax variations of C1, C2 and C3 components in the A1DOM, A2DOM and A3DOM; (e) the proportion of fluorescence components of the three MP-DOM. (C1: Photo-induced humic-like, C2: Terrestrial humic-like, C3: Plastic-derived protein/phenol-like.)

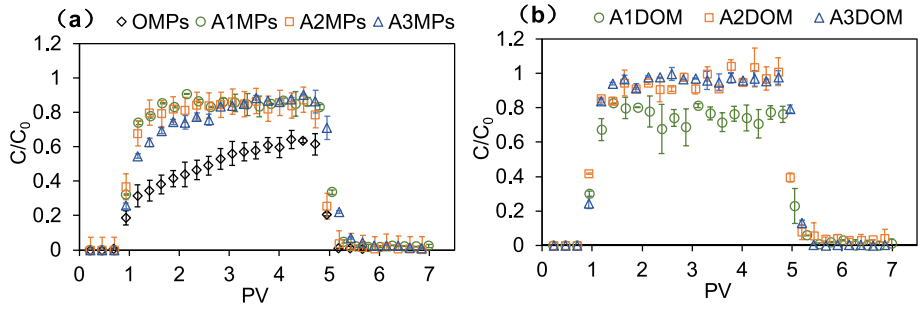

Fig. 3. Transport of the original MPs and A1, A2, A3-systems in saturated quartz sand porous media: breakthrough curves of MPs (a) and MP-DOM (b).

Adjusting the OMPs solution to pH = 3.95 led to a significant mobility reduction, with a recovery rate of only 21.3 % (Fig. S4). Consequently, the mobility difference between OMPs and AMPs becomes more pronounced. Thus, other mechanisms might be more important responsible for the increased mobility of AMPs. UV-aging process likely enhances -COOH group with much lower pK_a values on the MPs' surface, resulting in AMPs being deprotonated at relatively low pH (Liu et al., 2019b). Thus, the lower pH has less impact on the surface negativity of AMPs compared to OMPs. These increasing oxygen-functional groups on AMPs' surface likely enhance their hydrophilicity (Xu et al., 2022), reducing aggregation rates and increasing mobility (Liu et al., 2019b; Mao et al., 2020). Additionally, the reduction in particle size may contribute to the higher mobility of AMPs. Given that the migration ability of A1MPs has already increased to a very high level, further noticeable enhancement may require substantial property changes.

The migration ability of the three MP-DOM follows the order: A3DOM ≈ A2DOM > A1DOM. The varying concentrations of DOM (mg C/L) notably impacted MP-DOM transport. To elucidate this further, transport experiments were conducted by increasing the concentration of A1DOM to 15 mg C/L and decreasing A3DOM concentration to 4.7 mg

C/L (Fig. A10). Consequently, while the ERR of A3DOM decreased slightly from approximately 95 % to 90 %, the ERR of A1DOM experienced a notable increase, rising from roughly 80 % to 92 %. This trend indicates that the ERR of MP-DOM tends to increase with concentration. Additionally, even at the same concentration, A1DOM's mobility remained slightly weaker than A3DOM. Previous studies have confirmed that DOM with lower acidity and higher hydrophobicity is more prone to adsorption by a solid surface (Guo and Chorover, 2003; Liu et al., 2019a; Miao et al., 2022). In this study, A1DOM with the lowest acidity exhibited the greatest retention. It is widely known that contact angle positively correlates with the hydrophobicity of a liquid when the solid has a hydrophilic surface (e.g., SiO_2). Our measurements revealed contact angles of 50.5 ± 0.7°, 34.7 ± 0.6°, and 34.7 ± 1.2° between quartz plate and solutions of A1DOM, A2DOM, and A3DOM, respectively, suggesting a hydrophobicity order of A1DOM > A2DOM ≈ A3DOM, which corresponds to their retention in quartz sand. Furthermore, Lee et al. (2022) reported preferential adsorption between sand and protein/phenol-like C3 derived from UV-aged expanded PS. Thus, the highest relative intensity of C3 in A1DOM (Fig. S7) likely contributes to its enhanced retention.

Notably, as the aging degree increases, the TOC concentration of MP-DOM also rises. Given its high mobility, MP-DOM plays an increasingly significant role in the transport of secondary products derived from MPs in porous media. To better understand the TOC contributions of MP-DOM compared to of AMPs under environmentally relevant conditions, the A3-system, with the highest concentration of MP-DOM in this study, was selected as a representative for further investigations under varying ionic strengths, cation types, medium types, and medium grain sizes. Furthermore, the effect of MP-DOM and MPs on each other's transport behavior was examined using a series of experiments by effectively separating the MP-DOM and AMPs.

3.2. Co-transport of MP-DOM and AMPs

3.2.1. The effect of environmental factors on co-transport of MPs and MP-DOM

Fig. 4 presents the effects of ionic strengths and cation types (Na^+ and Ca^{2+}) on the transport of A3MPs and A3DOM in the A3 system, comparing their behavior to OMPs under similar conditions (column NO.1–6, 12–17). The migration of A3DOM was largely unaffected by these factors, with ERRs ranging from 91.8 % and 98.0 %. In contrast, A3MPs mitigation was more influenced by these variables, with inhibition increasing as IS rose. Specifically, Ca^{2+} had a more pronounced effect than Na^+, decreasing ERR from 77.1 % to 31.8 % for Ca^{2+} and from 83.2 % to 60.8 % for Na^+. However, the impact on A3MPs was much weaker compared to OMPs, with the ERR decreasing from 51.0 % to 0 for Na^+ and from 18.1 % to 0 for Ca^{2+} (Table 1). These results suggest that while IS significantly affects the migration of OMPs, its impact on their degradation products is notably weaker, particularly when considering MP-DOM's contribution.

Fig. 5 depicts the effects of medium types and medium grain sizes on the migration of A3MPs and A3DOM in A3 system, comparing these to OMPs under similar conditions (column NO.1, 7–9, 12, 18–20). The transport of A3DOM in coarse sand and medium sand exhibited no significant differences (ERRs of 95.2 % versus 92.8 %). However, the retention of A3DOM increased in fine sand, corresponding to an ERR of 55.8 %. While the transport of A3MPs and OMPs decreases with increasing grain size, a notable variation in migration is only observed in medium sand (ERRs of 81.2 % versus 51.0 %). This study detects limestone porous media as one of the highly prevalent and economical materials often used in permeable reactive barriers. The transport of A3MPs and OMPs in quartz sand differs significantly from that in limestone, with minimal amounts of A3MPs and OMPs detected in the effluent (ERRs of 6.0 % versus 8.3 %). The migration of A3DOM also decreased in limestone porous media, with an ERR of 83.8 %, which is relatively low. Unlike typical breakthrough behaviors in quartz sand, the breakthrough transport curve exhibited an asymmetric shape with a tailing effect. Li et al. (2023) found that limestone can effectively

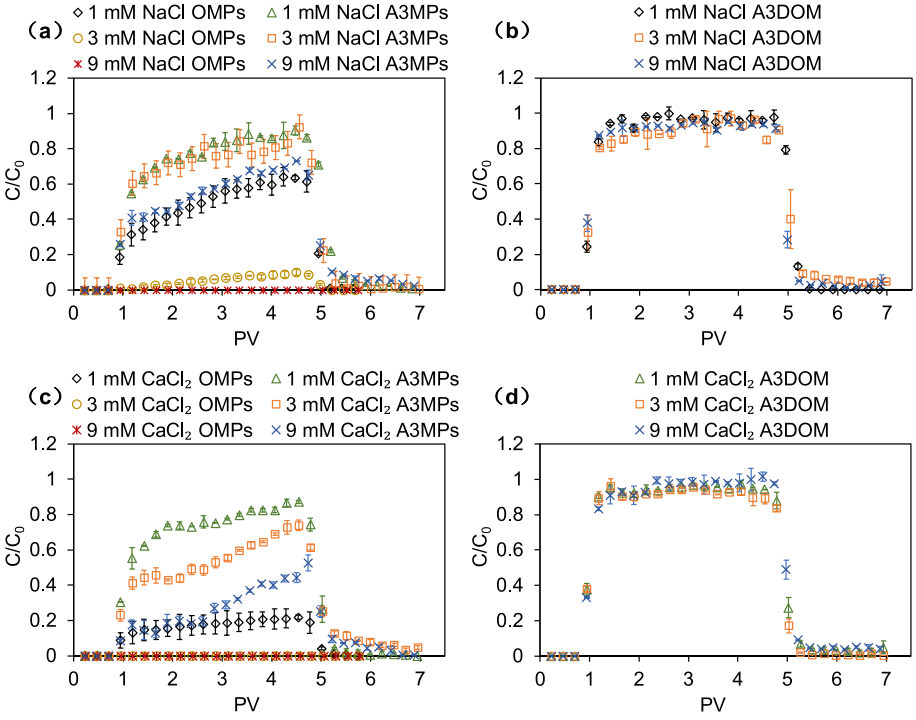

Fig. 4. Effect of concentration of NaCl (a, b) and $CaCl_2$ (c, d) on the transport of the original MPs and A3-system in saturated quartz sand porous media: breakthrough curves of MPs (a, c) and MP-DOM (b, d).

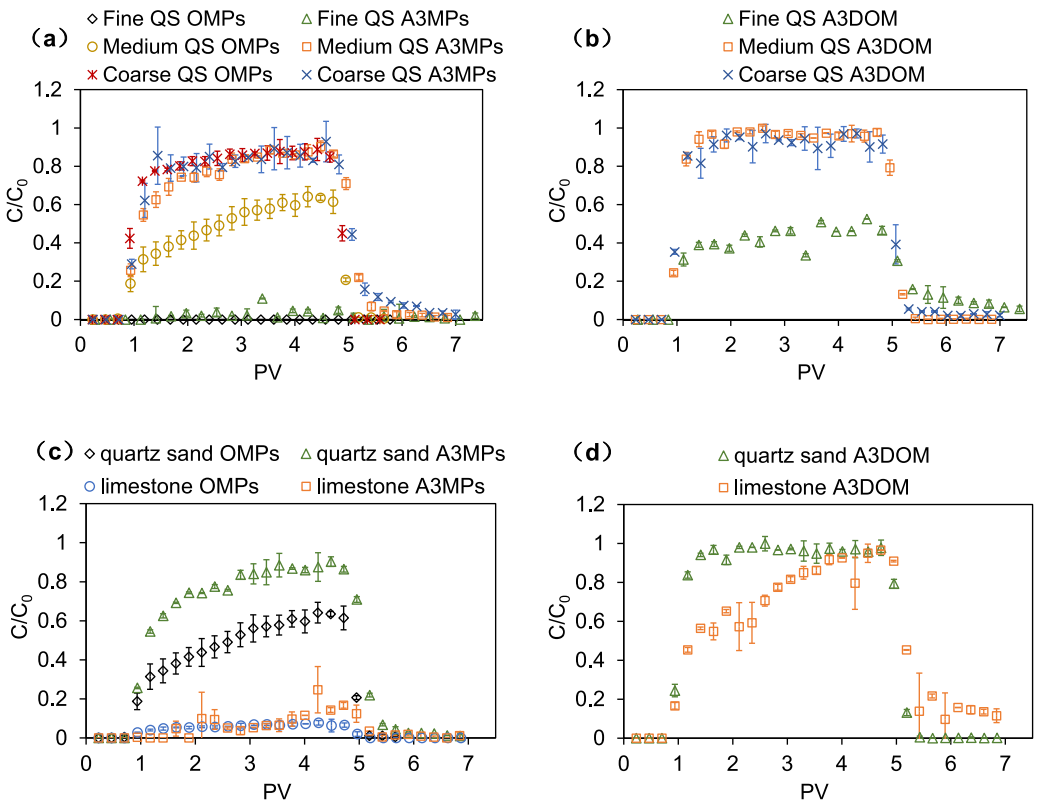

Fig. 5. Effect of grain size (a, b) and medium type (c, d), on the transport of the original MPs and A3-system in saturated porous media: breakthrough curves of MPs (a, c) and MP-DOM (b, d). (Quartz sand (QS) has a grain size that ranges from fine to coarse, including sizes of 0.250–0.355 (fine), 0.425–0.600 (medium) and 0.700–0.850 mm (coarse). The medium type encompasses quartz sand and limestone, all with the same grain size.)

remove pristine nanoplastics from wastewater when used in rapid sand filter systems of wastewater treatment plants. This study further suggests that limestone is also likely to remove aged ones well, but its removal of MP-DOM is limited.

As shown in Fig. 6 and Table 1, the proportion of A3DOM (mg C/L) increases while that of A3MPs decreases in the transport of degradation products under the tested conditions. Initially, the influent contains equal proportion of A3DOM and A3MPs (each 50 %). However, under all tested conditions excluding transport in fine sand, the proportion of A3DOM remains stable between 40 % and 50 %, whereas the proportion of A3MPs fluctuates significantly and is generally lower than that of A3DOM, ranging from 1 % to 40 %. In fine sand, the proportion of A3DOM drops to 29.26 % and A3MPs to 1.62 %, yet A3DOM remains the primary organic carbon component in the transport process. Therefore, the contribution of MP-DOM as part of degradation products to the transport process becomes more significant under diverse conditions.

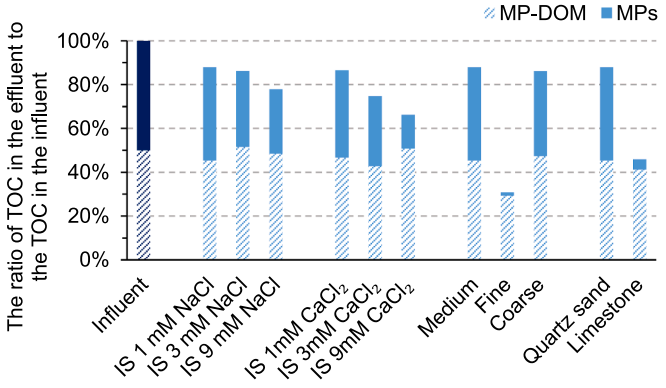

Fig. 6. The ratio of MP-DOM or MPs (mg C/L) in the effluent to the MP-DOM and MPs (mg C/L) in the influent under different tested conditions.

3.2.2. *Governing mechanisms*

The variations in electrostatic interaction between sand grains and A3MPs as well as between sand grains and OMPs under different concentrations of NaCl and $CaCl_2$ play a significant role in their differing migration behaviors. Specifically, Na^+ and Ca^{2+} ions could facilitate the deposition of particles through electrostatic screening effect in sand porous media (Zhao et al., 2020). As a divalent ion, Ca^{2+} exhibits a stronger screening effect compared to Na^+ (Mao et al., 2020). Table A3 shows that, with increasing IS of NaCl or $CaCl_2$, the decline in the zeta potential of A3MPs is smaller than that of OMPs. This smaller reduction in electrostatic repulsion between sand grains and A3MPs translates to higher mobility for A3MPs. Notably, the EER of A3MPs (31.8 %) in IS = 9 mM $CaCl_2$ solution were much higher than OMPs (18.1 %) in IS = 1 mM $CaCl_2$ solution. The zeta potential of OMPs in 1 mM $CaCl_2$ (−25.3 mV) was more negative than A3MPs in 9 mM $CaCl_2$ (−19.7 mV), and that of sand in 1 mM $CaCl_2$ (−15.5 mV) was more negative than in 9 mM $CaCl_2$ (−4.7 mV), indicating that electrostatic repulsion was not the only mechanism in controlling the transport behavior. Previous studies found that aging appeared to increase the resilience of PS nanoparticles mobility to the changes of solution chemistry (Liu et al., 2019b). UV-aging could produce charged groups and hydrophilic oligomers that enhance the colloidal stability of MPs in Ca^{2+} solutions, improving particle transport (Mao et al., 2020). Despite the wide range of zeta potential observed in sand under varying NaCl and $CaCl_2$ concentrations, the mobility of A3DOM did not remarkably change, indicating that the effect of electrostatic interaction on the mobility of A3DOM in quartz sand is quite low. The low molecular weight of A3DOM contributes to its high mobility. In this study, the A3DOM with all compounds having a molecular weight <1 kDa (A3DOM can pass through the 1 kDa membrane entirely). Similarly, Lee and Hur, 2020 reported

that the low-molecular-weight neutrals with a molecular weight <350 Da constituted the dominant fraction, ranging from 67.4 to 79.3 %, of the MP-DOM produced from PS under UV-light. The small hydrodynamic diameter of low molecular weight A3DOM help it resist aggregation in the presence of Ca^{2+} (Miao et al., 2022).

Colloid transport and retention behaviors depend strongly on the ratio of average particles diameter to median sand grain size. The ratios of average OMPs or A3MPs diameter to fine sand diameter (0.00166 or 0.00112) are approximate to the threshold value (~0.002–0.003), thus, straining plays a key role in colloid deposition in fine sand (Babakhani et al., 2017; Bradford et al., 2007). Enhanced colloid straining is observed with increasing particle-to-sand diameter ratios (Fig. 5a). For the high retention of A3DOM in fine sand, a possible explanation is that finer sand provides a higher specific surface area, offering more retention sites for A3DOM (Dong et al., 2016).

Limestone, with its buffering effect on pH, results in effluent pH values ranging from 7.4 to 7.8 across the columns, notably higher than those in quartz sand (where effluent pH was similar to influent pH). Conventionally, an increase in pH is believed to enhance the mobility of MPs in quartz sand porous media, both for original and aged ones, due to an increase in negative charge density on both MPs and quartz sand surface (Fei et al., 2022). However, in limestone porous media, opposite results were observed, with significant retention of MPs. The zeta potential of limestone is less negative compare to quartz sand (Table A2). This reduction in electrostatic repulsion likely contributes, to some extent, to the increased retention of OMPs and A3MPs. There are abundant Ca^{2+}, -COOH, and -OH on limestone surface (Figs. A5–6), which can significantly enhance the cation bridge effect, facilitating the adsorption of OMPs and A3MPs (Li et al., 2023). Additionally, A3DOM compounds containing -COOH and -OH may also be adsorbed onto the limestone surface through cation bridge by Ca^{2+} (Sun et al., 2019). Furthermore, the process of ligand exchange involves the binding of anions present in A3DOM, such as carboxyl groups, with the surface hydroxyl or carboxyl layers of the limestone. This interaction, driven by ligand exchange, plays a crucial role in the binding between these anionic groups of A3DOM and the hydroxyl on the surfaces (or edges) of limestone (Lee and Hur, 2020). The substantial release of Ca^{2+} from limestone have an inhibitory effect on MPs transport, primarily due to an increase in IS. Limestone could continuously release 0.2 mM Ca^{2+} steadily during the injection of background solution, and between 0.2 and 0.6 mM Ca^{2+} was released during the injection of A3MPs mixture (due to the acidic pH of A3MPs, about 3.5) (Fig. A7). The effluent resulting from the injection of DI-water (~pH 7) in the limestone was used as the background solution to investigate the transport of OMPs in quartz sand (Fig. A8). Finally, a ~ 40 % reduction in OMP recovery compared to DI-water as the background solution was observed. SEM images reveal that limestone has rougher surface than sand (Fig. A9). This rougher surface, with its potholes and holes, not only impedes shear flow and promotes the retention of OMPs and A3MPs (Li et al., 2023), but also possesses a larger specific surface area, offering more retention sites for A3DOM (Lyu et al., 2020; Sun et al., 2019).

3.3. Interactions between MPs and MP-DOM

Beyond the mechanisms controlling the transport and retention of original and aged MPs and MP-DOM, we interestingly found that MPs and MP-DOM are able to influence each other. As depicted in Fig. 7, the addition of A3DOM result in a decrease in pH (from 6.9 to 5.5), but still significantly promote the mobility of OMPs, and the recovery rate increase from 15.5 % to 65.0 %. When A3MPs are extracted and dispersed alone in background solution without any pH adjustment (pH = 5.5), the removal of A3DOM facilitates the transport of A3MPs, and the recovery rates increase from to 81.2 % to 89.2 %. When A3MPs are extracted and dispersed alone in background solution with a pH adjust to 3.6, which is similar to the A3-system, the presence of A3DOM exhibit a promotion in A3MPs transport. Obviously, A3DOM can promote OMPs transport more effectively than A3MPs, and the presence of A3MPs has minimal effect on A3DOM transport, with recovery rates of 95.2 % and 92.3 % for A3DOM alone and in mixture, respectively. However, the presence of OMPs slightly decreases A3DOM transport, with a recovery rate dropping to 87.2 %. We propose that A3DOM influences the transport of OMPs and A3MPs through a combination of positive and negative effects. The lower pH induced by A3DOM caused a protonation reaction of both the sand surface and nanoparticles, which result in a decrease in their negative charges. This further weakens their electrostatic repulsion and hinders MPs transport. In this interaction studies, the retention rate of A3DOM in quartz sand (Fig. 4b A3DOM alone) is 7.7 %, indicating that A3DOM possesses a certain adsorption capacity on quartz sand. Therefore, A3DOM can occupy some deposition sites on the media surface, resulting in competitive adsorption with MPs (Zhang et al., 2024a). The adsorption of 15 mg C/L A3DOM on 15 mg C/L OMPs (75.3 mg C/g C) is approximately twice as much as onto 15 mg C/L A3MPs (36.8 mg C/g C). This adsorption increases steric hindrance between MPs and quartz sand, potentially enhancing particle transport (Chen et al., 2012; Li et al., 2019; Zhang et al., 2024a). Taken together, we infer that the steric hindrance is likely more important to the OMPs than A3MPs. Meanwhile, A3DOM adsorbed on MPs cannot be filtered out, meaning a small portion of A3DOM is transported with MPs, resulting in breakthrough curves that slightly underestimate actual A3DOM transport, especially when mixed with OMPs.

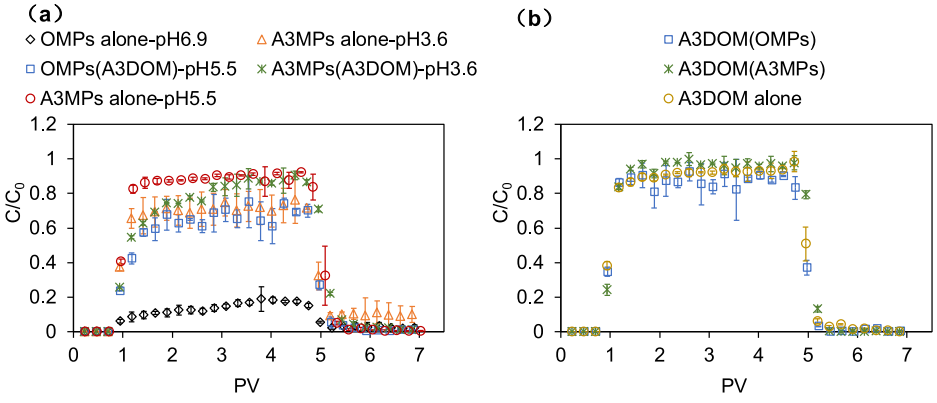

Fig. 7. The interaction between original/aged MPs and MP-DOM. (OMPs alone-pH 6.9: only 15 mg C/L OMPs; OMPs(A3DOM)/A3DOM(OMPs)-pH 5.5: 15 mg C/L OMPs +15 mg C/L A3DOM; A3MPs alone-pH 5.5: only 15 mg C/L A3MPs (the pH of A3MPs separated from the mixture that resuspended using DIW was higher than the A3MPs + A3DOM mixture); A3MPs alone-pH 3.6: only 15 mg C/L A3MPs (pH adjusted to 3.6 was conducted to avoid the adverse effect of lower pH on A3MPs transport); A3MPs(A3DOM)/A3DOM(A3MPs)-pH 3.6: 15 mg C/L A3MPs + 15 mg C/L A3DOM; A3DOM alone: only 15 mg C/L A3DOM.)

4. Conclusion

This is the first to explore the co-transport of MPs and MP-DOM simultaneously originating from UV-aged MPs in saturated porous media. Their co-transport behavior exhibited differences under various environmental conditions, including different IS, cation type, grain size, and medium type. Except in the mildest aging scenario, the transport capacity followed the order of MP-DOM > aged MPs > original MPs. MP-DOM as a degradation product in the co-transport process is particularly prominent due to its high mobility and significant proportion organic carbon within the system. In the quartz sand system, the enhanced transport of aged MPs was primarily due to the presence of oxygen-containing functional groups, which promoted the surface charge negativity and hydrophilicity. Hydrophilicity also plays a more significant role for the mobility of MP-DOM. Electrostatic interaction was not the primary mechanism for high MP-DOM transport, but it was for the retention of MPs under different IS and cation type. When the grain size of sand decreased to a certain value, the strong retention of aged MPs and MP-DOM could be attributed to the enhanced colloid straining and increased deposition sites. In the limestone system, the strong retention of aged MPs was attributed to cation bridging, increased IS from released Ca^{2+}, and surface roughness, while decreased MP-DOM transport resulted from cation bridging and ligand exchange. It is noteworthy that MPs and MP-DOM could influence each other, with the effect of MP-DOM on the transport of MPs being more significant than MPs on MP-DOM. MP-DOM affected the transport of MPs through a combination of positive (such as steric hindrance and competitive adsorption) and negative effects (including protonation, which is triggered by the acidic pH that MP-DOM provided).

5. Environmental implications

Microplastics aging causes a large amount of DOM to enter the subsurface environment. In addition to changing the pH and TOC of their surrounding environment, their high mobility, which is higher than that of MPs under various conditions, can expand the influence of plastic pollutants in soil-groundwater system. Furthermore, MP-DOM can affect the transport of MPs and potentially also the mobility of other particles (e.g., engineering nanoparticles or soil colloidal particles) in the subsurface environment. This study helps us to understand more deeply the effect of aging on the transport of MPs by considering the perspective of MP-DOM, and it facilitates a more comprehensive prediction of the risks associated with plastic aging.

CRediT authorship contribution statement

Kaixuan Sun: Writing – original draft, Investigation, Funding acquisition, Conceptualization. **Xiaofeng Huo:** Investigation. **Yanhong Zhang:** Supervision, Funding acquisition. **Chengyuan Zong:** Writing – review & editing. **Chao Liu:** Resources. **Zhanxue Sun:** Resources, Funding acquisition. **Xiaoxia Yu:** Writing – review & editing, Investigation. **Peng Liao:** Writing – review & editing.

Declaration of competing interest

The authors declare that they have no known competing financial interests or personal relationships that could have appeared to influence the work reported in this paper.

Appendix A. Supplementary data

Supplementary data to this article can be found online at https://doi.org/10.1016/j.scitotenv.2024.177597.

Data availability

Data will be made available on request.

References

Babakhani, P., Bridge, J., Doong, R.-A., Phenrat, T., 2017. Continuum-based models and concepts for the transport of nanoparticles in saturated porous media: a state-of-the-science review. Adv. Colloid Interface Sci. 246, 75–104. https://doi.org/10.1016/j.cis.2017.06.002.

Bradford, S.A., Torkzaban, S., Walker, S.L., 2007. Coupling of physical and chemical mechanisms of colloid straining in saturated porous media. Water Res. 41 (13), 3012–3024. https://doi.org/10.1016/j.watres.2007.03.030.

Castan, S., Henkel, C., Hüffer, T., Hofmann, T., 2021. Microplastics and nanoplastics barely enhance contaminant mobility in agricultural soils. Communications Earth & Environment 2 (1), 193–202. https://doi.org/10.1038/s43247-021-00267-8.

Chen, G., Liu, X., Su, C., 2012. Distinct effects of humic acid on transport and retention of TiO_2 rutile nanoparticles in saturated sand columns. Environ. Sci. Technol. 46 (13), 7142–7150. https://doi.org/10.1021/es204010g.

Dong, S., Gao, B., Sun, Y., Shi, X., Xu, H., Wu, J., Wu, J., 2016. Transport of sulfacetamide and levofloxacin in granular porous media under various conditions: experimental observations and model simulations. Sci. Total Environ. 573, 1630–1637. https://doi.org/10.1016/j.scitotenv.2016.09.164.

Fei, J., Xie, H., Zhao, Y., Zhou, X., Sun, H., Wang, N., Wang, J., Yin, X., 2022. Transport of degradable/nondegradable and aged microplastics in porous media: effects of physicochemical factors. Sci. Total Environ. 851, 158099–158109. https://doi.org/10.1016/j.scitotenv.2022.158099.

Gewert, B., Plassmann, M., Sandblom, O., MacLeod, M., 2018. Identification of chain scission products released to water by plastic exposed to ultraviolet light. Environ. Sci. Technol. Lett. 5 (5), 272–276. https://doi.org/10.1021/acs.estlett.8b00119.

Geyer, R., Jambeck, J.R., Law, K.L., 2017. Production, use, and fate of all plastics ever made. Sci. Adv. 3 (7), 1–5. https://doi.org/10.1126/sciadv.1700782.

Guo, M., Chorover, J., 2003. Transport and fractionation of dissolved organic matter in soil columns. Soil Sci. 168 (2), 108–118. https://doi.org/10.1097/00010694-200302000-00005.

Kwon, B.G., Koizumi, K., Chung, S.-Y., Kodera, Y., Kim, J.-O., Saido, K., 2015. Global styrene oligomers monitoring as new chemical contamination from polystyrene plastic marine pollution. J. Hazard. Mater. 300, 359–367. https://doi.org/10.1016/j.jhazmat.2015.07.039.

Lee, Y.K., Hur, J., 2020. Adsorption of microplastic-derived organic matter onto minerals. Water Res. 187, 116426–116438. https://doi.org/10.1016/j.watres.2020.116426.

Lee, Y.K., Murphy, K.R., Hur, J., 2020. Fluorescence signatures of dissolved organic matter leached from microplastics: polymers and additives. Environ. Sci. Technol. 54 (19), 11905–11914. https://doi.org/10.1021/acs.est.0c00942.

Lee, Y.K., Hong, S., Hur, J., 2021. A fluorescence indicator for source discrimination between microplastic-derived dissolved organic matter and aquatic natural organic matter. Water Res. 207, 117833–117842. https://doi.org/10.1016/j.watres.2021.117833.

Lee, Y.K., Yoo, H.-Y., Ko, K.-S., He, W., Karanfil, T., Hur, J., 2022. Tracing microplastic (MP)-derived dissolved organic matter in the infiltration of MP-contaminated sand system and its disinfection byproducts formation. Water Res. 221, 118806–118816. https://doi.org/10.1016/j.watres.2022.118806.

Lee, Y.K., He, W., Guo, H., Karanfil, T., Hur, J., 2023. Effects of organic additives on spectroscopic and molecular-level features of photo-induced dissolved organic matter from microplastics. Water Res. 242, 120272–120284. https://doi.org/10.1016/j.watres.2023.120272.

Li, J., Chen, J., Lu, T., Wang, Y., Zhang, H., Shang, Z., Li, D., Zhou, Y., Qi, Z., 2019. Effects of low-molecular weight organic acids on the transport of graphene oxide nanoparticles in saturated sand columns. Sci. Total Environ. 666, 94–102. https://doi.org/10.1016/j.scitotenv.2019.02.242.

Li, X., Zhang, Y., Xu, H., Sun, Y., Gao, B., Wu, J., 2023. Granular limestone amended sand filters for enhanced removal of nanoplastics from water: performance and mechanisms. Water Res. 229, 119443–119451. https://doi.org/10.1016/j.watres.2022.119443.

Liu, F., Xu, B., He, Y., Brookes, P.C., Xu, J., 2019a. Co-transport of phenanthrene and pentachlorophenol by natural soil nanoparticles through saturated sand columns. Environ. Pollut. 249, 406–413. https://doi.org/10.1016/j.envpol.2019.03.052.

Liu, J., Zhang, T., Tian, L., Liu, X., Qi, Z., Ma, Y., Ji, R., Chen, W., 2019b. Aging significantly affects mobility and contaminant-mobilizing ability of nanoplastics in saturated loamy sand. Environ. Sci. Technol. 53 (10), 5805–5815. https://doi.org/10.1021/acs.est.9b00787.

Liu, P., Lu, K., Li, J., Wu, X., Qian, L., Wang, M., Gao, S., 2020. Effect of aging on adsorption behavior of polystyrene microplastics for pharmaceuticals: adsorption mechanism and role of aging intermediates. J. Hazard. Mater. 384, 121193–121202. https://doi.org/10.1016/j.jhazmat.2019.121193.

Liu, P., Li, H., Wu, J., Wu, X., Shi, Y., Yang, Z., Huang, K., Guo, X., Gao, S., 2022. Polystyrene microplastics accelerated photodegradation of co-existed polypropylene via photosensitization of polymer itself and released organic compounds. Water Res. 214, 118209–118219. https://doi.org/10.1016/j.watres.2022.118209.

Lyu, X., Liu, X., Sun, Y., Gao, B., Ji, R., Wu, J., Xue, Y., 2020. Importance of surface roughness on perfluorooctanoic acid (PFOA) transport in unsaturated porous media. Environ. Pollut. 266. https://doi.org/10.1016/j.envpol.2020.115343, 115343–11551.

Mao, Y., Li, H., Huangfu, X., Liu, Y., He, Q., 2020. Nanoplastics display strong stability in aqueous environments: insights from aggregation behaviour and theoretical calculations. Environ. Pollut. 258, 113760–113770. https://doi.org/10.1016/j.envpol.2019.113760.

Miao, C., Zhou, H., Lv, Y., Shang, J., Mamut, A., 2022. Combined effects of ferrihydrite coating and ionic type on the transport of compost-derived dissolved organic matter in saturated porous media. Environ. Pollut. 307, 119501–119509. https://doi.org/10.1016/j.envpol.2022.119501.

Ouyang, Z., Li, S., Xue, J., Liao, J., Xiao, C., Zhang, H., Li, X., Liu, P., Hu, S., Guo, X., Zhu, L., 2023. Dissolved organic matter derived from biodegradable microplastic promotes photo-aging of coexisting microplastics and alters microbial metabolism. J. Hazard. Mater. 445, 130564–130575. https://doi.org/10.1016/j.jhazmat.2022.130564.

Ren, Z., Gui, X., Wei, Y., Chen, X., Xu, X., Zhao, L., Qiu, H., Cao, X., 2021a. Chemical and photo-initiated aging enhances transport risk of microplastics in saturated soils: key factors, mechanisms, and modeling. Water Res. 202, 117407–117416. https://doi.org/10.1016/j.watres.2021.117407.

Ren, Z., Gui, X., Xu, X., Zhao, L., Qiu, H., Cao, X., 2021b. Microplastics in the soil-groundwater environment: aging, migration, and co-transport of contaminants – a critical review. J. Hazard. Mater. 419, 126455–126467. https://doi.org/10.1016/j.jhazmat.2021.126455.

Ren, X., Han, Y., Zhao, H., Zhang, Z., Tsui, T.-H., Wang, Q., 2023. Elucidating the characteristic of leachates released from microplastics under different aging conditions: perspectives of dissolved organic carbon fingerprints and nano-plastics. Water Res. 233, 119786–119795. https://doi.org/10.1016/j.watres.2023.119786.

Rillig, M.C., 2018. Microplastic disguising as soil carbon storage. Environ. Sci. Technol. 52 (11), 6079–6080. https://doi.org/10.1021/acs.est.8b02338.

Rillig, M.C., Leifheit, E., Lehmann, J., 2021. Microplastic effects on carbon cycling processes in soils. PLoS Biol. 19 (3), 1–9. https://doi.org/10.1371/journal.pbio.3001130.

Shi, Y., Liu, P., Wu, X., Shi, H., Huang, H., Wang, H., Gao, S., 2021. Insight into chain scission and release profiles from photodegradation of polycarbonate microplastics. Water Res. 195, 116980–116990. https://doi.org/10.1016/j.watres.2021.116980.

Siddiqui, S.A., Singh, S., Bahmid, N.A., Shyu, D.J.H., Domínguez, R., Lorenzo, J.M., Pereira, J.A.M., Câmara, J.S., 2023. Polystyrene microplastic particles in the food chain: characteristics and toxicity - a review. Sci. Total Environ. 892, 164531–164541. https://doi.org/10.1016/j.scitotenv.2023.164531.

Sun, K., Sun, Y., Gao, B., Xu, H., Wu, J., 2019. Effect of cation type in mixed Ca-Na systems on transport of sulfonamide antibiotics in saturated limestone porous media. Environ. Sci. Pollut. Res. 26 (11), 11170–11178. https://doi.org/10.1007/s11356-019-04561-z.

Sun, Y., Li, X., Li, X., Wang, J., 2022. Deciphering the fingerprint of dissolved organic matter in the soil amended with biodegradable and conventional microplastics based on optical and molecular signatures. Environ. Sci. Technol. 56 (22), 15746–15759. https://doi.org/10.1021/acs.est.2c06258.

Thompson, R.C., Olsen, Y., Mitchell, R.P., Davis, A., Rowland, S.J., John, A.W.G., McGonigle, D., Russell, A.E., 2004. Lost at sea: where is all the plastic? Science 304 (5672), 838. https://doi.org/10.1126/science.1094559.

Tian, L., Chen, Q., Jiang, W., Wang, L., Xie, H., Kalogerakis, N., Ma, Y., Ji, R., 2019. A carbon-14 radiotracer-based study on the phototransformation of polystyrene nanoplastics in water versus in air. Environ. Sci. Nano 6 (9), 2907–2917. https://doi.org/10.1039/c9en00662a.

Wang, H., Zhu, J., He, Y., Wang, J., Zeng, N., Zhan, X., 2023. Photoaging process and mechanism of four commonly commercial microplastics. J. Hazard. Mater. 451, 131151–131163. https://doi.org/10.1016/j.jhazmat.2023.131151.

Xi, X., Wang, L., Zhou, T., Yin, J., Sun, H., Yin, X., Wang, N., 2022. Effects of physicochemical factors on the transport of aged polystyrene nanoparticles in saturated porous media. Chemosphere 289, 133239–133249. https://doi.org/10.1016/j.chemosphere.2021.133239.

Xu, Y., Ou, Q., Li, X., Wang, X., van der Hoek, J.P., Liu, G., 2022. Combined effects of photoaging and natural organic matter on the colloidal stability of nanoplastics in aquatic environments. Water Res. 226, 119313–119323. https://doi.org/10.1016/j.watres.2022.119313.

Zhang, G., Cui, J., Song, J., Ji, Y., Zuo, Y., Jia, H., Yin, X., 2024a. Transport of polystyrene nanoplastics with different functional groups in goethite-coated saturated porous media: effects of low molecular weight organic acids and physicochemical properties. J. Colloid Interface Sci. 653, 423–433. https://doi.org/10.1016/j.jcis.2023.09.090.

Zhang, Y., Ding, G., Zhao, Z., Gao, S., Li, L., Feng, Q., Farooq, U., Lu, T., Chen, W., Qi, Z., 2024b. Insight into the effects of low-molecular-weight aromatic acids on biochar colloid-assisted transport of Cd^{2+} through saturated porous media. Colloids Surf. A Physicochem. Eng. Asp. 133306-133317. https://doi.org/10.1016/j.colsurfa.2024.133306.

Zhao, W., Zhao, P., Tian, Y., Shen, C., Li, Z., Peng, P., Jin, C., 2020. Investigation for synergies of ionic strength and flow velocity on colloidal-sized microplastic transport and deposition in porous media using the colloidal–AFM probe. Langmuir 36 (22), 6292–6303. https://doi.org/10.1021/acs.langmuir.0c00116.

Zhou, J.J., Zhang, Z.N., Xiong, J.Q., Shi, W.P., Liang, L.P., Zhang, F.H., Zhang, F., 2023. Nitrogen removal performance of bioretention cells under polyethylene (PE) microplastic stress. Environ. Pollut. 338, 122655–122663. https://doi.org/10.1016/j.envpol.2023.122655.

Update

Science of the Total Environment

Volume 957, Issue , 20 December 2024, Page

DOI: https://doi.org/10.1016/j.scitotenv.2024.177935

Science of the Total Environment 957 (2024) 177935

Contents lists available at ScienceDirect

Science of the Total Environment

journal homepage: www.elsevier.com/locate/scitotenv

Corrigendum

Corrigendum to "Mechanistic insights into the co-transport of microplastic degradation products in saturated porous media: The key role of microplastics-derived DOM" [Sci. Total Environ. 957(2024)/177597]

Kaixuan Sun [a], Xiaofeng Huo [b], Yanhong Zhang [b,*], Chengyuan Zong [c], Chao Liu [a], Zhanxue Sun [a], Xiaoxia Yu [a,*], Peng Liao [d]

[a] Jiangxi Provincial Key Laboratory of Genesis and Remediation of Groundwater Pollution, East China University of Technology, Nanchang 330013, Jiangxi, PR China
[b] School of Water Resources and Environmental Engineering, East China University of Technology, NanChang 330013, Jiangxi, PR China
[c] Zhejiang Environmental Technology Co., Ltd, Hangzhou 310012, PR China
[d] State Key Laboratory of Environmental Geochemistry, Institute of Geochemistry, Chinese Academy of Sciences, Guiyang 550081, PR China

The authors regret that the printed version of the above article omitted the acknowledgements. It is as follows:

Acknowledgements

This work was financially supported by the Natural Science Foundation of Jiangxi Province (20232BAB213089, 20232BAB203078), Doctoral Start-up Foundation of East China University of Technology (1410000715), National Natural Science Foundation of China (42107093, 51861145308), the Science and Technology Research Project of Jiangxi Provincial Education Department (GJJ2200761).

The authors would like to apologise for any inconvenience caused.

DOI of original article: https://doi.org/10.1016/j.scitotenv.2024.177597.
* Corresponding authors.
E-mail addresses: 201660015@ecut.edu.cn (Y. Zhang), yuxiaoxiayxx@126.com (X. Yu).

https://doi.org/10.1016/j.scitotenv.2024.177935

Available online 8 December 2024